

Experimental evidence of waves in the sublayer

By W. R. B. MORRISON,† K. J. BULLOCK

Department of Mechanical Engineering, University of Queensland, Australia

AND R. E. KRONAUER

Harvard University, Cambridge, Mass., U.S.A.

(Received 28 April 1970 and in revised form 8 January 1971)

Two-dimensional frequency-wave-number spectra $\Phi(k_x, \omega)$ and $\Phi(k_z, \omega)$ of the longitudinal velocity component are presented for the sublayer in fully developed turbulent pipe flow, at Reynolds numbers between 10 600 and 46 400. All of these sublayer spectra apparently scale by introducing dimensionless quantities based on a characteristic length scale ν/U_τ and a characteristic time scale ν/U_τ^2 .

Representative convection velocities have been obtained from the $\Phi(k_x, \omega)$ spectra. The characteristic convection velocity in the sublayer is independent of wave-number and is the same at all positions in the layer $c_x \simeq 8.0U_\tau$. This result has led to the conclusion that sublayer turbulence is wave-like.

Existing visualization data seem to indicate that the sublayer waves are also relatively periodic at least at low values of Reynolds number. Characteristic dimensions of the sublayer waves are $\lambda_x^+ \simeq 630$, and $\lambda_z^+ = 135$. Results of the visualization studies of Fage & Townend (1932) and of Runstadler, Kline & Reynolds (1963) and Kline *et al.* (1967) do not appear to conflict with a wave model for the sublayer.

All of the existing measurements of the sublayer have been for relatively low Reynolds numbers. Some of the present results for positions just outside the sublayer suggest that at Reynolds numbers greater than 30 000, the structure and properties will change substantially from those observed to date. In particular the streaky structure which is commonly regarded as being characteristic of the sublayer will probably not be detected at sufficiently high Reynolds numbers.

Introduction

The viscous sublayer has been the subject of numerous experimental and theoretical investigations and many models of its structure have been proposed. One of the earliest observations was made by Fage & Townend (1932) using an ultramicroscope. They found that the sublayer was not truly laminar and that the ratio of the (r.m.s.) velocity fluctuation, to the mean velocity, reached a maximum near the pipe wall.

Hot-wire measurements of Laufer (1954) also demonstrated that the sublayer was not laminar but more importantly they showed that the production and

† Present address: Oceanics Australia, Brisbane, Australia

dissipation of the turbulence reached maximum values in the vicinity of the sublayer edge.

Einstein & Li (1956) studied the sublayer by injecting dye at the wall of a pipe. They observed that dye filaments after moving along the wall would suddenly erupt into the bulk of the flow and from this they postulated that the sublayer periodically grew and decayed. An erupting sublayer model was also proposed independently by Hanratty (1956).

The most detailed visualization data for the sublayer has been collected by workers from Stanford University. Kline & Runstadler (1959) used dye injection techniques and Runstadler, Kline & Reynolds (1963) used a hydrogen bubble method as did Schraub *et al.* (1965). Their most important observation was that the sublayer exhibited a remarkably regular and almost periodic variation in velocity across the flow. Within the sublayer the dye or hydrogen bubbles contracted to form regularly spaced 'streaks' of low velocity fluid. These streaks were found to move slowly away from the wall as they progressed downstream, undergoing transverse oscillations. Some of these streaks were ejected into the bulk of the flow.

A common feature of many of the models proposed for the flow in the sublayer and wall adjacent regions is a streamwise vortex attached to the wall. Such eddies were first suggested by Townsend (1956) as being the dominant large eddy in the flow. Runstadler *et al.* (1963) noted that the streak breakup process which occurs outside the sublayer was associated with longitudinal vorticity and in a report of a recent study of the viscous sublayer in a pipe, Bakewell & Lumley (1967) suggest that contrarotating pairs of streamwise vortices are the predominant feature of the sublayer and adjacent region.

The propagation of wave disturbances in the sublayer has been studied analytically (Sternberg 1962, 1965; Schubert & Corcos 1967). In all cases, however, the concept was one of a turbulence field external to the sublayer 'driving' the oscillations of the sublayer, and the analyses are valid only for a wave speed well in excess of the local fluid velocity. The wave disturbances described here convect with a characteristic velocity which matches the fluid velocity near the edge of the sublayer itself and cannot be described by these theories. It should be noted that the calculations of Schubert & Corcos give a turbulence velocity component normal to the wall in the sublayer almost two orders of magnitude below that which is experimentally observed. The explanation is that the calculations were performed for wave disturbances whose characteristic size was matched to the dominant structure in the log-layer. In fact, to achieve the observed magnitude for this velocity component it is necessary that the waves be of the small size described here. †

The dimensions of the zone termed the sublayer are not universally accepted but the edge is generally taken to be at a value of y^+ between 5 and 10. Thus the

† This follows simply from the continuity equation. Since the normal component of turbulence is zero at the wall, in order for it to attain its observed magnitude at $y^+ = 12$ (approximately $\frac{1}{2}U_\tau$) the turbulence velocity parallel to the surface must have a large divergence in that plane. Since this parallel component is about five times as large as the normal component a dominant wave-number, $k\nu/U_\tau$, of order 0.05 can be inferred.

thickness of the layer is in general very small and the finite size of a transducer makes the experimental investigation of the sublayer very difficult. One commonly accepted way of increasing the thickness of the layer is to reduce the Reynolds number of the flow. However, it is then impossible to be sure that the results found will apply to larger Reynolds numbers. In fact the majority of all sublayer investigations (including the investigation reported here) have been for quite small Reynolds numbers and it is likely that the characteristics of the sublayer identified to date are only characteristic of low Reynolds number flow. Some of the results presented here seem to confirm this view.

Some new measurements in the sublayer

The sublayer measurements described here were made in air, in a tube of 5.24 in. inside diameter, at a position 64 diameters from the inlet. At the test section the flow was turbulent and fully developed. The measurements form part of a much larger experimental programme which was designed to investigate flow structure in the wall region of pipe flow.

Two-dimensional frequency-wave-number spectra, $\Phi(k_x, \omega)$ and $\Phi(k_z, \omega)$, of the longitudinal velocity component were measured, being generated† by Fourier transforming narrow band spatial correlations $R_u(x)$ and $R_u(z)$. These correlation functions were obtained using two hot-wire anemometer probes and two constant-current hot-wire anemometers. The hot wires were located at the same distance y from the wall, separated by distances x or z in the longitudinal or transverse directions respectively. The wires were normal to the mean flow and thus measured the longitudinal velocity fluctuations u . Further details of the experimental techniques and the complete results are described by Morrison (1969). Some of the two-dimensional spectra results reported here have been presented previously in another context by Morrison & Kronauer (1969).

All spectral densities are presented here as products of power density and the corresponding wave-number and frequency. Two-dimensional spectra, for instance, are presented as quantities $\mathcal{P}(k_x, \omega)$ or $\mathcal{P}(k_z, \omega)$ defined as

$$\begin{aligned}\mathcal{P}(k_x, \omega) &= k_x \cdot \omega \cdot \Phi(k_x, \omega), \\ \mathcal{P}(k_z, \omega) &= k_z \cdot \omega \cdot \Phi(k_z, \omega).\end{aligned}$$

One reason for adopting this type of presentation is that the significant ranges of k_x , k_z and ω span several decades and need therefore to be plotted on logarithmic scales. If linear scales are used for the spectral densities $\mathcal{P}(k_x, \omega)$ and $\mathcal{P}(k_z, \omega)$ the energy in a particular frequency-wave-number band is directly proportional to the volume under the spectrum in this band and may be assessed directly.

† Two-dimensional spectra generated this way are restricted to one quadrant (positive k and ω for example) and they represent disturbances with both positive and negative convection velocities (see, for example, Wills 1964). In the case of $\Phi(k_z, \omega)$ this does not matter because the energy in disturbances propagating in either z direction must be equal from symmetry considerations. $\Phi(k_x, \omega)$, on the other hand, represents mainly disturbances propagating downstream but includes a small unknown component due to disturbances propagating upstream. Disturbances travelling upstream can be separated by measuring the quadrature spectra.

In addition the spectra used here are normalized so that the total volume is unity and

$$\iint_0^\infty \Phi(k_x, \omega) dk_x d\omega = \iint_{-\infty}^\infty \mathcal{P}(k_x, \omega) d \ln k_x d \ln \omega = 1.0.$$

Two-dimensional spectra also provide an appropriate basis for the definition of convection velocity (see Wills 1964). A point (k, ω) in frequency-wave-number space can be associated with a phase velocity c of ω/k . Where two-dimensional spectra are presented with frequency and wave-number on logarithmic scales, then lines of constant convection velocity are straight lines of unit slope. A characteristic convection velocity which can be associated with a particular wave-number or a particular frequency is defined here from the co-ordinates of the 'ridge line' of $\mathcal{P}(k, \omega)$, on a $\ln \omega, \ln k$ plot.

All of the quantities used in the presentation of the results have been made dimensionless by introducing appropriate length and time scales. In doing this it has been assumed that the sublayer is controlled by the shear velocity U_τ and the kinematic viscosity ν so that the length scale used is ν/U_τ and the time scale is ν/U_τ^2 . The following dimensionless variables are used:

$$\begin{aligned} y^+ &= yU_\tau/\nu; & \omega^+ &= \omega\nu/U_\tau^2; \\ c_x^+ &= c_x/U_\tau; & c_z^+ &= c_z/U_\tau; \\ k_x^+ &= k_x\nu/U_\tau = \omega^+/c_x^+; & k_z^+ &= k_z\nu/U_\tau; \\ \lambda_x^+ &= \lambda_x U_\tau/\nu; & \lambda_z^+ &= \lambda_z U_\tau/\nu. \end{aligned}$$

The two-dimensional spectral density results for the sublayer positions are shown in figures 1-7 and the flow conditions corresponding to these results are given in table 1.

$Re = U_c a/\nu$	U_τ (ft/sec)	y (in.)	y/a	y^+
		$\mathcal{P}(k_x, \omega)$ data		
10 700	0.43	0.007	0.00257	1.56
17 100	0.60	0.010	0.00382	2.96
		0.020	0.00763	5.92
46 400	1.48	0.010	0.00382	7.30
		$\mathcal{P}(k_x, \omega)$ data		
10 500	0.43	0.007	0.00257	1.52
17 100	0.58	0.010	0.00382	2.96
		0.020	0.00763	5.93

U_c = centre-line velocity. a = radius of the tube 2.62 in.

TABLE 1. Flow conditions corresponding to two-dimensional spectra measurements in the sublayer

Characteristic properties of the sublayer

The available data show that the use of viscid scaling in the sublayer may be appropriate since the two-dimensional spectra $\mathcal{P}(k_x^+, \omega^+)$ (figures 1-3) and $\mathcal{P}(k_z^+, \omega^+)$ (figures 5-7) both seem to be unique functions for the region. However, $\mathcal{P}(k_z^+, \omega^+)$ at $y^+ = 7.3$ (figure 4) exhibits distinct deviations at low frequencies and low wave-numbers. The deviations at this y^+ could be due to the proximity of the sublayer edge, but it is more likely that they are due to a Reynolds number effect and this is discussed later.

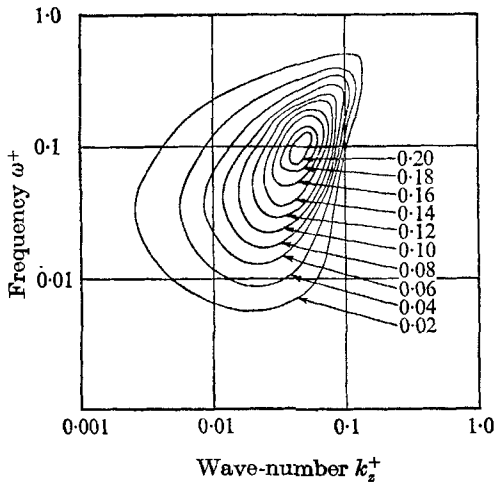


FIGURE 1. Two-dimensional spectra $\mathcal{P}(k_z^+, \omega^+)$ for $Re = 10\,700$, $y^+ = 1.56$.

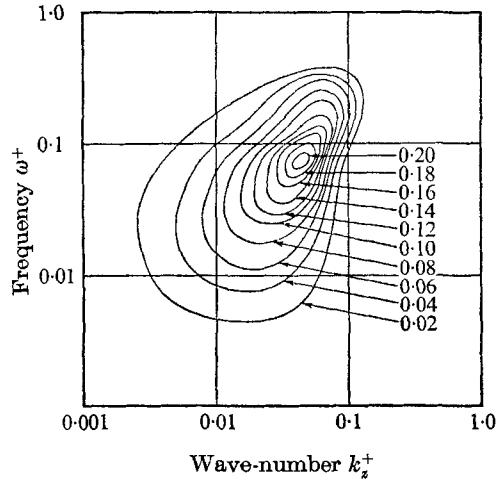


FIGURE 2. Two-dimensional spectra $\mathcal{P}(k_z^+, \omega^+)$ for $Re = 17\,100$, $y^+ = 2.96$.

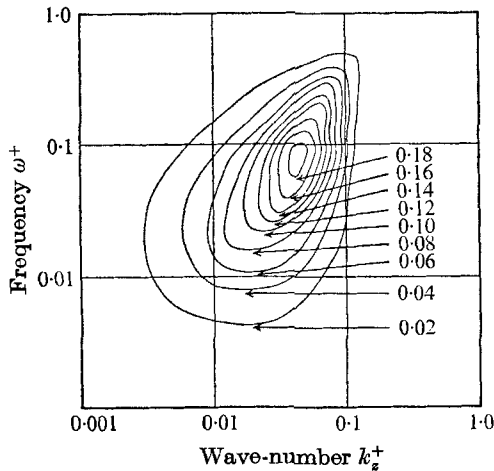


FIGURE 3. Two-dimensional spectra $\mathcal{P}(k_z^+, \omega^+)$ for $Re = 17\,100$, $y^+ = 5.92$.

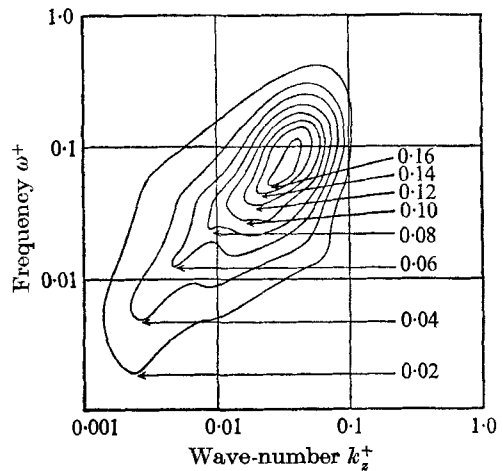


FIGURE 4. Two-dimensional spectra $\mathcal{P}(k_z^+, \omega^+)$ for $Re = 46\,400$, $y^+ = 7.3$.

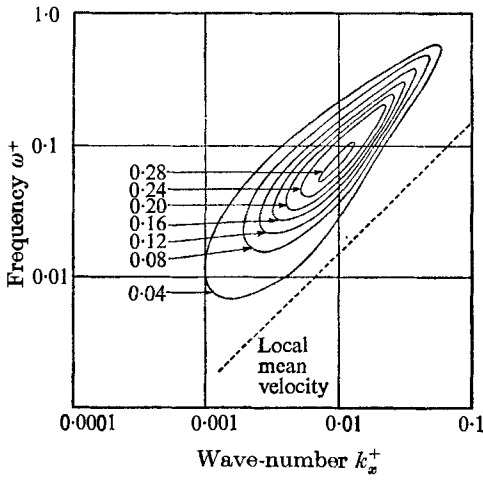


FIGURE 5. Two-dimensional spectra $\mathcal{P}(k_x^+, \omega^+)$ for $Re = 10\,500$, $y^+ = 1.52$.

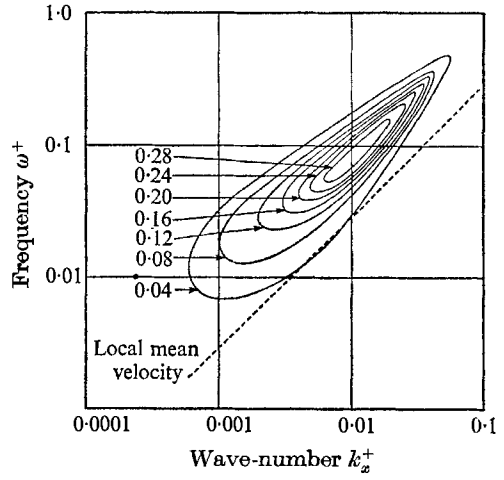


FIGURE 6. Two-dimensional spectra $\mathcal{P}(k_x^+, \omega^+)$ for $Re = 17\,100$, $y^+ = 2.96$.

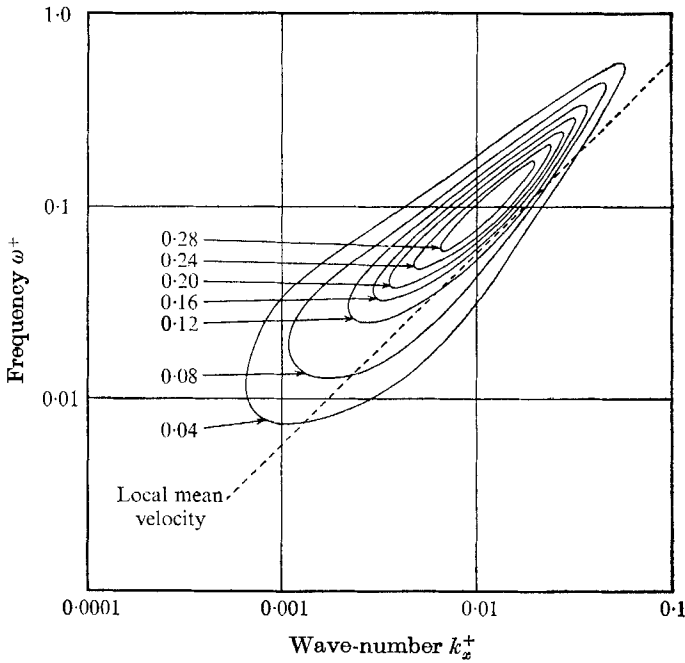


FIGURE 7. Two-dimensional spectra $\mathcal{P}(k_x^+, \omega^+)$ for $Re = 17\,100$, $y^+ = 5.93$.

If for the moment the sublayer is regarded as being independent of Reynolds number then it is possible to assign characteristic dimensions corresponding to the maxima of $\mathcal{P}(k_x^+, \omega^+)$ and $\mathcal{P}(k_z^+, \omega^+)$. The following approximate values are obtained:

$$k_z^+ = 0.047, \quad \lambda_z^+ = 135, \dagger$$

$$k_x^+ = 0.010, \quad \lambda_x^+ = 630.$$

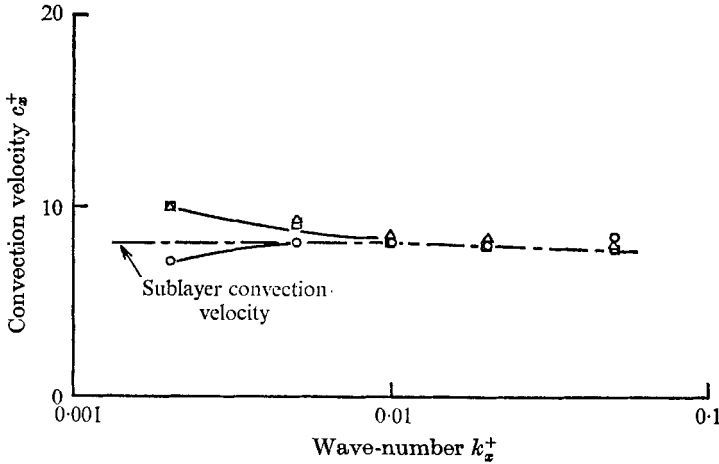


FIGURE 8. Non-dimensional convection velocities in the sublayer.

	y^+	U_r (ft/sec)	Re
○	1.52	0.43	10 500
□	2.96	0.58	17 100
△	5.93	0.58	17 100

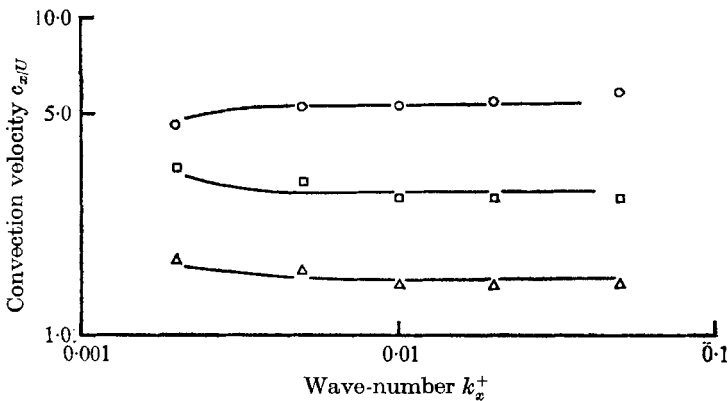


FIGURE 9. Convection velocities in the sublayer normalized on mean stream velocities. Symbols same as figure 8.

The transverse wave-number is relatively well defined since the 'ridge line' of the $\mathcal{P}(k_z^+, \omega^+)$ plots tends to be almost parallel to the ω^+ axis. On the other hand, the $\mathcal{P}(k_x^+, \omega^+)$ plots are concentrated about lines of constant convection velocity so that the longitudinal wavelength is only weakly defined. In fact the

† The value of transverse wavelength agrees remarkably well with the most recent estimate of streak spacing given by Kline *et al.* (1967) as $\lambda_z^+ = 130$.

$\mathcal{P}(k_x^+, \omega^+)$ plots are centred on the one convection velocity. There is, of course, a reasonable spread in the observed values but this is identically repeated at all positions in the layer.

To demonstrate the trend in convection velocity more clearly, specific values have been obtained from the $\mathcal{P}(k_x^+, \omega)$ plots (using the co-ordinates of the ridge line of $\mathcal{P}(k_x^+, \omega)$) and replotted showing c_x^+ as a function of wave-number k_x^+ . The data is presented at c_x^+ in figure 8 and as c_x^+/U (normalized on the local mean velocity) in figure 9. Because c_x^+ is relatively constant (approximately $c_x^+ = 8.0$) c_x^+ is greater than the local mean velocity for positions close to the wall. At the closest position to the wall ($y^+ = 1.56$) disturbances on the average travel at about five times the local mean velocity and an examination of figure 5 shows that at least 99% of the turbulent energy is accounted for by disturbances propagating at speeds at least twice the local velocity.

Because the convection velocity c_x^+ and the longitudinal wave-number k_x^+ (for maximum P) are relatively constant, it is also possible to assign a characteristic frequency ω^+ to the sublayer. The present results indicate a value of $\omega^+ = 0.07$ for this frequency.

From the estimates of transverse and longitudinal wavelengths λ_z^+ and λ_x^+ it is possible to calculate an average angle of propagation for disturbances. If β is the angle between the disturbance wave front and the flow direction then $\tan \beta = \lambda_z^+/\lambda_x^+$ and an average value for the sublayer would be $\tan \beta \simeq 0.21$, $\beta \simeq 12^\circ$.† Sublayer disturbances are therefore quite steeply inclined to the flow.

Wave model for the sublayer

The longitudinal turbulent velocity field at a given y , $u(x, z, t)$, is a random function which is statistically stationary in all of its arguments. Taking Fourier transforms of u with respect to these arguments (or transforms of the correlations of u) leads to a mathematical description of the velocity field as a sum of wave components which may not necessarily have any special physical relevance. A wave, in a physical sense, must have the periodic motions co-ordinated at different y locations. To demonstrate this co-ordination unambiguously would require measurements of u to be made simultaneously at different y , i.e. an experimental programme an order of magnitude more extensive than that reported here.

What the data here show is that at all y throughout the sublayer the spectral composition of the u velocity field is virtually identical. In particular, the disturbances close to the wall possess a dominant phase velocity of $8U_r$ which corresponds to the average fluid velocity at $y^+ \simeq 9$. Add to this the well-known fact that the root-mean-square magnitude of the u fluctuations is so large (30% of local mean velocity) that large displacements of fluid normal to the surface are surely taking place. It is then highly probable that the fluctuations of u are strongly co-ordinated throughout the sublayer. In fact it is difficult to conceive of any mechanism that would produce disturbances at $y^+ = 1$ propagating at a

† Care should be exercised in assigning any real physical relevance to this value.

phase velocity of $8U_\tau$ which does not couple such disturbances with events much further out in the sublayer.

If the spectral power were sharply concentrated at some particular ω , k_x , k_z set, then it would be possible to characterize the sublayer disturbances as a simple harmonic wave of a particular size, inclination and speed. Actually the spectral power is spread out and as a result the waves cover a range of sizes, inclinations and speeds. Of these three the most sharply defined is the speed, since almost two-thirds of the power is concentrated in a range of speeds between $6U_\tau$ and $12U_\tau$. The property next most sharply defined is the size of the waves, which is related to the total wave-number, k_{tot} ,

$$k_{tot} = (k_x^2 + k_z^2)^{\frac{1}{2}}.$$

Now, since k_x^2 is found to be typically an order of magnitude smaller than k_z^2 it follows that the size of the waves is given closely by $2\pi/k_z$. Then from figures 1–3 it is seen that more than two-thirds of the wave power lies in a wave size range of about 4:1. The range of wave inclinations (which can be estimated from the range of the ratio of ω^+ to k_x^+) is seen to cover at least a decade.

It was observed earlier that considerations of symmetry lead to the expectation of waves propagating with equal ease in positive and negative circumferential directions. Waves of both types will generally be occurring simultaneously and it is worth considering the visual aspect that this combination will present. If, for simplicity, we consider two pure harmonic waves with the same ω and k_x , but with k_z of opposite sign, an equal combination of these will generate a wave pattern which is 'standing' in the z co-ordinate but propagating in x with a velocity ω/k_x . Then at a fixed x location, the appearance will be that of a temporally modulated periodic structure in z displaying no obvious propagation in z . Of course such precise symmetry is improbable and the actual appearance would contain some mixture of standing and propagating waves.

Review of existing visualization data

It is interesting to review the existing visualization data for two reasons; first to see how well these results support a wave model for the sublayer, and secondly to examine why it is that propagation velocities very much greater than the local mean have not previously been detected.

Before examining the data it is well to have fixed in mind the kind of results which would be expected if the turbulence motions are wave-like and how they compare with the motions which would be observed for a stationary pattern of streamwise eddies. Figure 10(a) is a sketch of the stationary streamwise eddy flow with alternate regions of upwelling and downwelling. The characteristic features of this flow are large cyclic excursions of particles toward and away from the walls, and virtually no time variation of velocity at any fixed point in the flow. Figure 10(b) shows the secondary motions which would be seen at a fixed station x if the periodicity in z is generated by two equal waves propagating in opposite z directions. Within this pattern, points located a distance $\frac{1}{2}\lambda_z$ apart oscillate out of phase. Similarly, shifting to a station downstream a distance $\frac{1}{2}\lambda_x$

will produce an identical pattern but with a shift of π in temporal phase. In comparing figures 10(a) and 10(b) it should be noted that both flows represent co-ordinated motions throughout the sublayer, but since the wave pattern is oscillatory, the transverse displacements of fluid particles can be expected to be much less than the λ_z^+ which characterizes the pattern as a whole.

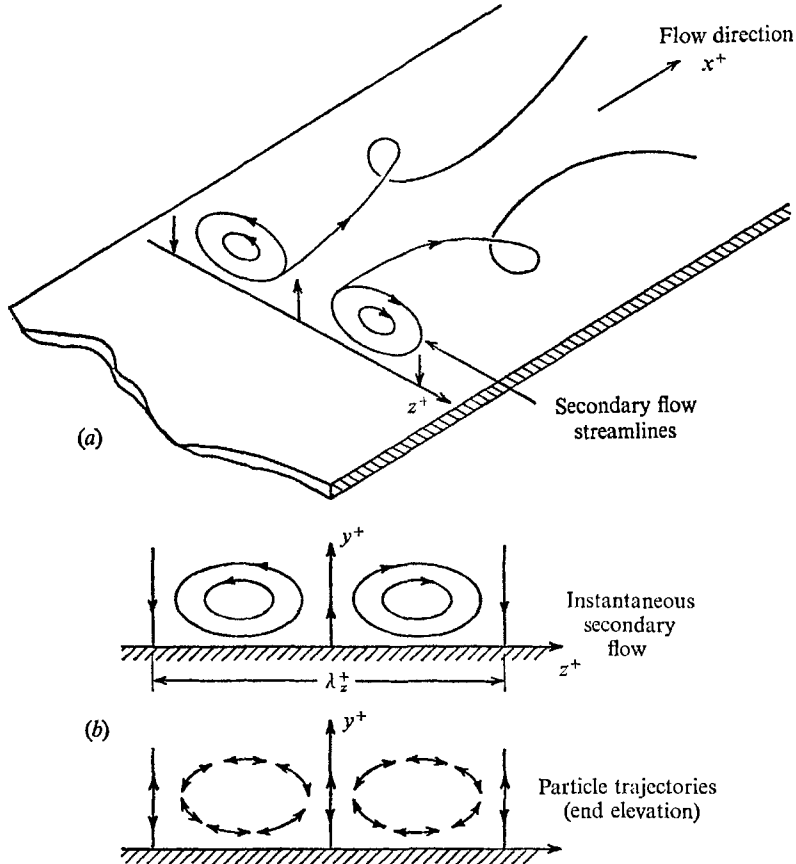


FIGURE 10. (a) Stationary streamwise eddies. (b) Secondary motions in a temporally modulated standing wave pattern.



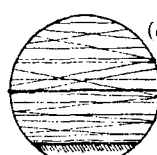
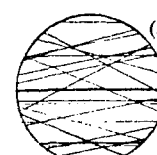
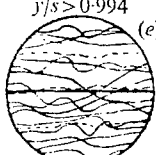
Stationary objective				
Flow at centre of pipe $y/s=0$		Flow at $y/s=0.95$		Flow very close to wall $y/s > 0.994$
				
Laminar	Turbulent $\theta = \pm 7^\circ$	Flow normal to wall, $\theta_{xy} = \pm 10^\circ$	Flow parallel to wall, $\theta_{xz} = \pm 27^\circ$	Flow parallel to wall, θ_{xz} of order $\pm 70^\circ$

FIGURE 11. Visualization results of Fage & Townend (1932).

Consider now the relevant results of Fage & Townend (1932) reproduced in figure 11. Clearly for positions very near the wall particle motions are quite periodic. This cannot be ascribed to circulation about a stationary vortex because with the large displacements required normal to the wall the particles would pass out of focus. Assuming then that the motion is due to the passage of waves through the sublayer, individual tracer particles will follow roughly sinusoidal paths, but the wavelength of this particle motion, λ_{px} , (indicated by the pathlines) will in general be different from the actual wavelength λ_x of the basic wave disturbance. The ratio of λ_{px} to λ_x will simply be the ratio of the local mean velocity, U , to the convection velocity c_x .†

In this data the lines sketched are pathlines only and there is nothing to indicate the dimensions of the basic wave motions. From their data at the position closest to the wall it is possible to estimate an average particle motion wavelength of $\lambda_{px}^+ \simeq 6.0$, whereas the average wavelength λ_x estimated from the (k_x^+, ω^+) data presented here is $\lambda_x^+ \simeq 630$. It is, however, possible to calculate λ_x^+ from Fage & Townend's results by estimating an average mean velocity which would correspond to their data closest the wall (all particles less than $y^+ = 0.4$ were in focus) and by assuming that the convection velocity for disturbance is $8.0U_r$ as suggested by the present results. Using a value of $u^+ = 0.2$ then $\lambda_x^+ = \lambda_{px}^+ \cdot c_x^+ / u^+ \simeq 240$, which is at least of the same order of magnitude as the value obtained here from the two-dimensional spectra.

The hydrogen bubble and dye injection studies reported by Runstadler *et al.* (1963) and Kline *et al.* (1967) must be considered differently, since each photographic frame is a collection of streaklines and not particle paths. Typical hydrogen bubble photographs from Kline *et al.* (1967)‡ are reproduced in figure 12 (plate 1) and a typical dye filament photograph which has been extracted from the movie film by Runstadler *et al.* (1963) is reproduced in figure 13 (plate 2). First consider the events occurring just at the marker source when it is deep in the sublayer. A motion of the fluid toward the solid boundary at some point on the marker line is accompanied by: (i) a longitudinal velocity higher than the local mean because high velocity fluid is being brought down from further out, and (ii) a divergence of the secondary flow field when viewed toward the wall. The opposite effects occur when fluid moves outward from the solid boundary; the longitudinal velocity is reduced and the tracers are converged into the characteristic distinct streak. All of these are clearly visible at the hydrogen bubble wire in figure 12. For reasons which will soon be detailed, it is best not to use the name 'streak' for this region of marker convergence, but rather 'concentration zone'.

Next consider the subsequent history of the fluid in the concentration zone. It will move downstream slowly (compared with the longitudinal wave speed of $8U_r$) and as the wave field moves past events will reverse themselves. That is,

† It is feasible to make the distinction between λ_{px} and λ_x from a movie film if combined time and streak markers are used, but the analysis is quite tedious and is virtually impossible by eye in real time.

‡ Actually only three of these photographs appears in the published paper. The photograph for $y^+ = 6.6$ was kindly supplied by Professor Kline.

the concentration zone will at a later time be in a region of transverse spreading flow which disperses the tracer. Of course complete reversal is impossible and evidence of the original concentration will remain, but in a ragged form. At the same time new concentration zones are being laid down at the wire in between the original locations. In an idealized regular and symmetrical wave field the concentration pattern should look like figure 14(a). If, however, the wave propagating in one direction were to be temporarily stronger than the opposite

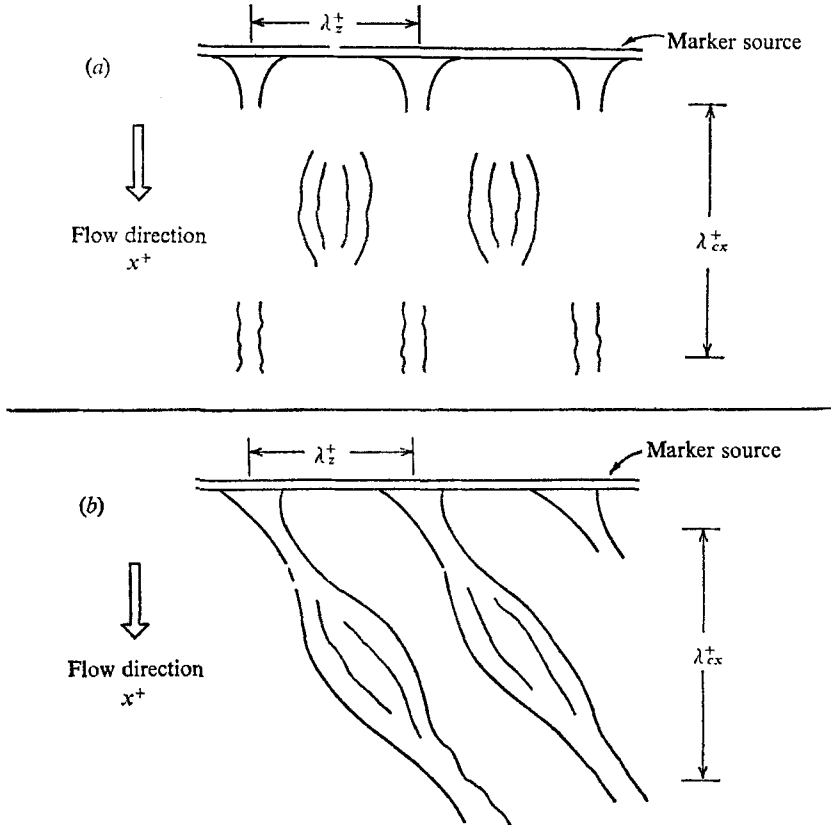


FIGURE 14. Pattern of concentration zones for (a) a symmetrical wave system; (b) a non-symmetrical wave system.

propagating wave, the pattern would look like figure 14(b). The $y^+ = 2.7$ photograph of figure 12, and sections of figure 13 show evidence of the behaviour sketched in figure 14(a). The $y^+ = 4.5$ photograph of figure 12 resembles figure 14(a), only on the right side, and resembles figure 14(b) on the left side.

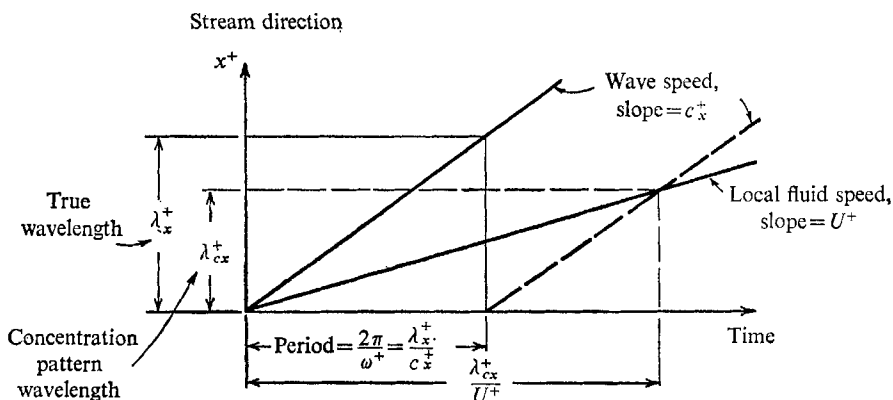
The kinematic relationships necessary to interpret concentration diagrams are naturally different from those used in particle path diagrams. Figure 15 is a propagation diagram from which it is concluded that the ratio of the longitudinal wavelength seen in the concentration diagram, λ_{cx}^+ to the true wavelength is given by

$$\frac{\lambda_{cx}^+}{\lambda_x^+} = \frac{U^+}{c_x^+ - U^+}$$

Applying this to the $y^+ = 4.5$ photograph of figure 12 with $U^+ \simeq 4U_\tau$ and $c_x^+ \simeq 8U_\tau$ it follows that the apparent longitudinal wavelength is very close to the true λ_x^+ . From the slope of the streaks in the left side of this photograph, $\lambda_{cx}^+ \simeq 5\lambda_z^+$ which is in excellent agreement with the data reported here. For the $y^+ = 2.7$ photograph it would be expected that

$$\lambda_{cx}^+ = \frac{2.7}{8 - 2.7} \lambda_x^+ \simeq \frac{1}{2} \lambda_x^+ \simeq 2.5 \lambda_z^+.$$

There is some weak evidence to support this ratio.



$$\frac{\lambda_{cx}^+}{U^+} - \frac{\lambda_x^+}{c_x^+} = \frac{\lambda_x^+}{c_x^+}$$

FIGURE 15. Propagation diagram for waves in the sublayer.

Figure 13 provides a better example of the concentration patterns than figure 12 because the dye provides a denser and therefore more persistent marker than hydrogen bubbles. At one side of the flow $\lambda_{cx}^+ \simeq 7\lambda_z^+$ and at the other side it is about $9\lambda_z^+$. Using $\lambda_x^+ = 5\lambda_z^+$ and working backward through the kinematic relation for $\lambda_{cx}^+/\lambda_x^+$ gives c_x^+/U^+ of $12/7$ and $14/9$ respectively. For $c_x^+ = 8U_\tau$ this implies U/U_τ (i.e. y^+) of 4.7 and 5.1 . While the dominant y^+ location of the dye being photographed is not known accurately, other figures in that report (numbered 35c and 35d) show dye 'streaks' at y^+ of about 5. Also, the authors state (page 55) that 'streaks' form in the wall layers, $0 < y^+ \leq 10$, and for the most part break up in the zone $10 < y^+ < 40$.

Note that in the formation of concentration patterns there are two conflicting effects at work. Since the turbulence has $c_x^+ \simeq 8U_\tau$, the wave centres are near $y^+ = 9$. Thus, while there may be large displacements of fluid normal to the wall at this y^+ there will be very little of the spanwise flow, necessary to produce marker concentration (cf. figure 10(b)). This is confirmed in the figure 12 sequence where the concentrations are noticeably most weak at $y^+ = 9.6$. On the other hand, at very low y^+ where the wave speed is most different from the local fluid

speed and λ_{cz}^+ is very small, the pattern will not persist very far in the stream direction. Therefore, concentration patterns which are both strong and persistent must be found at intermediate y^+ (say, 4 to 6).

It is important to note that a single line in the inclined concentration pattern of figure 14(b) is *not* made up of fluid passing by a single point on the bubble line and therefore is not a streak line. By misinterpreting such a line to be a streakline it is easy to find evidence for stationary streamwise eddies in a flow field where they do not in fact exist.

Before leaving the visualization data, some comments on the existence of streamwise vorticity are in order. Both the stationary streamwise eddy and the wave pattern contain regions of a strong vorticity in the centres of the secondary circulation. The important difference between the two cases is that the vorticity oscillates and periodically reverses sign in the wave pattern. The concentration zones in the wave pattern are regions of very low vorticity at all times.

Runstadler *et al.* (1963) made a particular effort to detect vorticity in concentration zones, mainly to support a previous postulate (Kline & Runstadler 1959). It is not surprising that they were forced to conclude "However the interpretation of the streak formation and break-up in terms of vortices is neither confirmed nor denied. Study of the flow in the streaks prior to the break-up when the pattern was as large as it could be made. . . *did not show any clear evidence of vorticity in the streak* prior to break-up. Thus the swirling in break-up may be due to the nature of the interaction process in break-up rather than to the streak pattern itself."

Effect of Reynolds number

Virtually all of the existing measurements and visualization studies of the sublayer including the results described here have been made for very low Reynolds numbers (see table 2). It is quite probable that the characteristics and dimensions of the sublayer which have been observed to date may only apply for these low Reynolds numbers. Indeed some of the results of the present study which were taken at positions just outside the sublayer tend to indicate that the

Author	Re	U_τ (ft/sec)	Fluid
Fage & Townend (1932)	3400	0.061	Water
Laufer (1954)	25000	0.42	Air
Einstein & Li (1956)	3850	0.024	Water
Kline (1967)	11100	0.0145	Water
Bakewell & Lumley (1967)	4350	1.28	Glycerine
Present data	10700	0.43	Air
	17100	0.60	
	46400	1.48	

$$Re = U_c a / \nu \text{ for a pipe, } a = \text{pipe radius, } U_c = \text{centre-line velocity;} \\ = U_\infty \delta / \nu \text{ for boundary layer.}$$

TABLE 2

character of the sublayer will change radically at Reynolds numbers above about 30 000. Two-dimensional power spectra $\mathcal{P}(k_x^+, \omega)$ are presented in figures 16 and 17 for positions at virtually the same y^+ ($y^+ = 14.6$ and 13.9) but at two different Reynolds numbers (46 400 and 96 500). By comparing these two results it can be seen that increasing the Reynolds number has had the effect of increasing

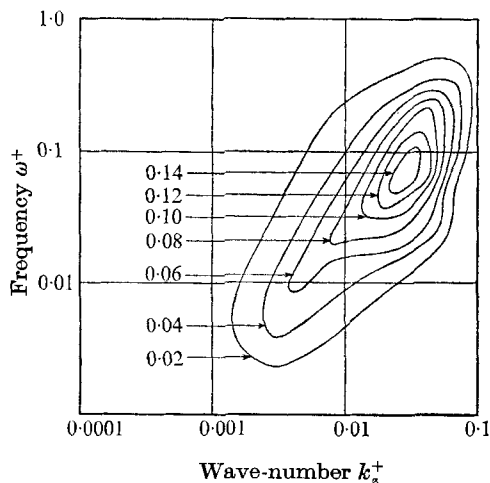


FIGURE 16. Two-dimensional power spectra $\mathcal{P}(k_x^+, \omega^+)$ for $Re = 46\,400$, $y^+ = 14.6$.

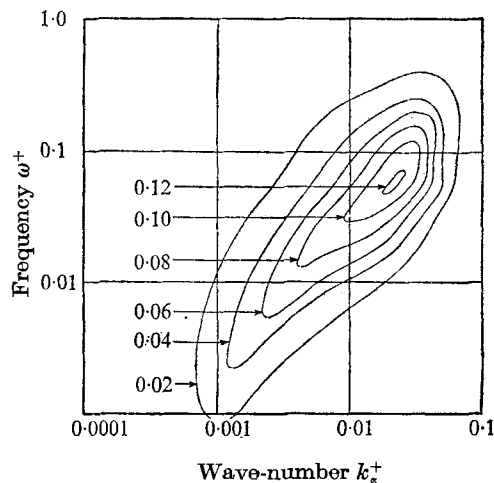


FIGURE 17. Two-dimensional power spectra $\mathcal{P}(k_x^+, \omega^+)$ for $Re = 96\,500$, $y^+ = 13.9$.

the relative amount of low frequency, low wave-number (k_x^+) energy. Most probably this additional energy will also appear within the sublayer itself and evidence for this is contained in figures 16 and 4. These latter $\mathcal{P}(k_x^+, \omega)$ are for the same Reynolds number and it can be seen that the distribution of energy at the sublayer edge ($y^+ = 14.6$) is very little different from the distribution within the layer ($y^+ = 7.3$). It seems very likely that figure 4 differs from that of figures 1–3 because of a Reynolds number effect and not because figure 4 corresponds to a position closer to the sublayer edge. The universality of shape of $\mathcal{P}(k_x^+, \omega^+)$ and $\mathcal{P}(k_x^+, \omega)$ and of various one-dimensional spectra as observed by Morrison (1969) and Bakewell & Lumley (1967) may be a feature of the sublayer only at low Reynolds numbers.

The additional low frequency, low wave-number energy which becomes significant at higher Reynolds numbers results from disturbances which convect at velocities much greater than the characteristic sublayer velocity ($8.0U_\tau$). This can be seen from figure 18 where $\mathcal{P}(k_x^+, \omega^+)$ at $y^+ = 14.6$ is presented. The low frequency, low wave-number energy has an average convection velocity of about $16U_\tau$.

If the sublayer acquires a broader range of wave-numbers as the Reynolds number is raised, a significant change in visualization patterns can be expected. In particular the ‘streaky’ structure of the sublayer as observed by Runstadler *et al.* (1963) (which undoubtedly is related to the low Reynolds number $\mathcal{P}(k_x^+, \omega^+)$,

$\mathcal{P}(k_x^+, \omega^+)$ data presented here) will probably become less important as Reynolds number increases and they may become completely indistinguishable at sufficiently high values.

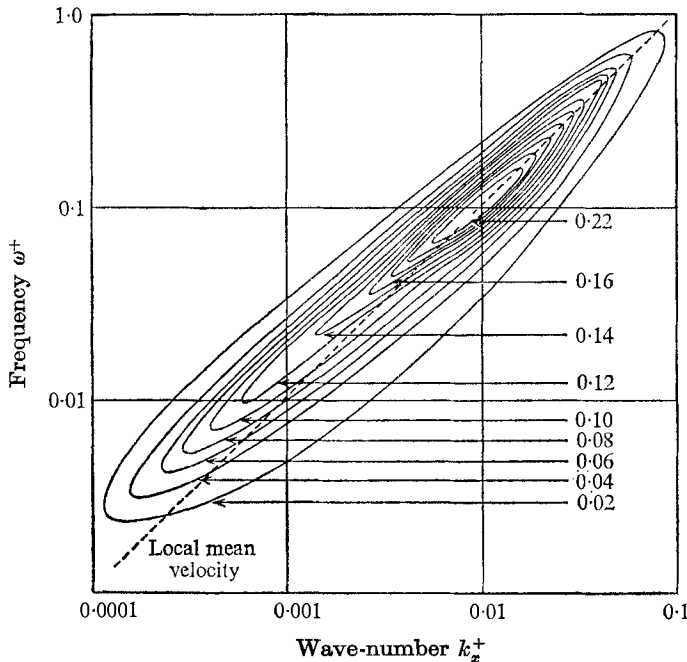


FIGURE 18. Two-dimensional power spectra $\mathcal{P}(k_x^+, \omega^+)$ for $Re = 46400$, $y^+ = 14.6$.

Conclusions

At low Reynolds numbers it is appropriate to scale turbulence quantities in the sublayer by introducing a characteristic length scale of ν/U_τ and a characteristic time scale of ν/U_τ^2 . This means that two-dimensional and one-dimensional spectra when appropriately scaled are universal functions for the sublayer.

Two-dimensional $\mathcal{P}(k_x^+, \omega^+)$ spectra indicate that the convection velocity is constant throughout the sublayer and this result requires that disturbances in the sublayer must be wave-like. In fact at low Reynolds numbers it is likely that the sublayer consists of relatively periodic waves. These waves propagate equally in both transverse directions and from existing visualization data seem to be limited in spatial extent, probably to something less than three to four wavelengths.

It is possible to specify average properties for the sublayer waves from the two-dimensional $\mathcal{P}(k_x^+, \omega^+)$ and $\mathcal{P}(k_y^+, \omega^+)$ spectra, and the following characteristic values have been estimated:

longitudinal wavelength	$\lambda_{x_1}^+ = 630$;
transverse wavelength	$\lambda_y^+ = 135$;
convection velocity	$c_x^+ = 8.0$;
critical layer height	$y_0^+ \simeq 9.0$.

The value of transverse wavelength agrees very well with the latest estimate of streak spacing for a zero-pressure gradient boundary layer given by Kline *et al.* (1967) as $\lambda_g^+ = 130$.

A review of the visualization studies reported by Fage & Townend (1932), Runstadler *et al.* (1963) and Kline (1967) seems to indicate that a wave model for the sublayer would not conflict with any of these results. Average wave properties estimated from these data agree tolerably well with the values obtained here.

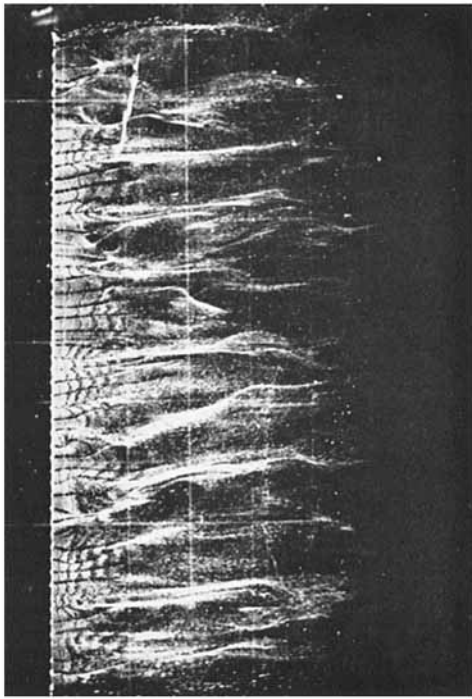
All of the properties and characteristics of the sublayer observed to date have been for low Reynolds number flows. There is evidence in the present results that at higher Reynolds numbers (probably greater than about 30 000) the character of the sublayer will be substantially altered, with an increasing amount of low frequency, low wave-number energy being introduced. The disturbances responsible for this additional energy have propagation velocities much larger than that which characterizes the sublayer at low Reynolds numbers. The 'streaky' structure which has been assumed to be characteristic of the sublayer will become less important as Reynolds number is increased and it is probable that the 'streaks' may not be apparent at all at sufficiently large values.

This work has been sponsored by the Australian Institute of Nuclear Science and Engineering and by Rothmans of Pall Mall (Aust.) and their assistance is gratefully acknowledged.

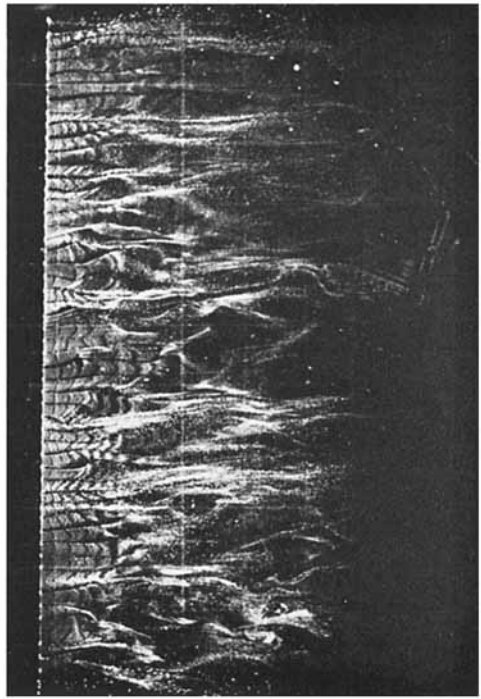
REFERENCES

- BAKEWELL, H. P. & LUMLEY, J. L. 1967 Viscous sublayer and adjacent wall region in turbulent pipe flow. *Phys. Fluids*, **10**, 1880.
- EINSTEIN, H. A. & LI, H. 1956 The viscous sublayer along a smooth boundary. *Am. Soc. Civil Engrs Proc.* **82**, 945.
- FAGE, A. & TOWNEND, H. C. H. 1932 An examination of turbulent flow with an ultra-microscope. *Proc. Roy. Soc. A* **135**, 656.
- HANRATTY, T. J. 1956 Turbulent exchange of mass and momentum with a boundary. *J. Am. Inst. Chem. Engrs*, **2**, 359.
- KLINE, S. J. 1967 Observed structure features in turbulent and transitional boundary layers. *Gen. Motors Symposium on Internal Flow*. Amsterdam: Elsevier.
- KLINE, S. J., REYNOLDS, W. C., SCHRAUB, F. A. & RUNSTADLER, P. W. 1967 The structure of turbulent boundary layers. *J. Fluid Mech.* **30**, 741.
- KLINE, S. J. & RUNSTADLER, P. W. 1959 Some preliminary results of visual studies of wall layers of the turbulent boundary layer. *ASME Trans. J. Appl. Mech.* 166.
- LAUFER, J. 1954 The structure of turbulence in fully developed pipe flow. *NACA Rep.* 1174.
- MORRISON, W. R. B. 1969 Two-dimensional frequency-wavenumber spectra and narrow band shear stress correlations in turbulent pipe flow. Ph.D. thesis, Department of Mechanical Engineering, University of Queensland.
- MORRISON, W. R. B. & KRONAUER, R. E. 1969 Structural similarity for fully developed turbulence in smooth tubes. *J. Fluid Mech.* **39**, 117.
- RUNSTADLER, P. W., KLINE, S. J. & REYNOLDS, W. C. 1963 An experimental investigation of the flow structure of the turbulent boundary layer. *Rep. MD-8, Thermo-sciences Div., Mech. Engr. Dep., Stanford University*.

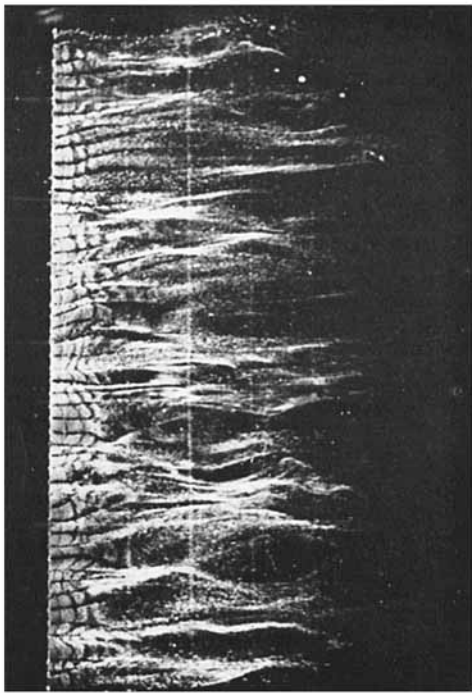
- SCHRAUB, F. A., KLINE, S. J., HENRY, J., RUNSTADLER, P. W. & LITTLE, A. 1965 Use of hydrogen bubbles for quantitative determination of time dependent velocity fields in low speed water flows. *ASME Trans. J. Basic Eng.* 429.
- SCHUBERT, G. & CORCOS, G. M. 1967 The dynamics of turbulence near a wall according to a linear model. *J. Fluid Mech.* **29**, 113.
- STERNBERG, J. 1962 A theory for the viscous sublayer of a turbulent flow. *J. Fluid Mech.* **13**, 241.
- STERNBERG, J. 1965 *AGARDOGRAPH* 97 (1st Paper).
- TOWNSEND, A. A. 1956 *The Structure of Turbulent Shear Flow*. Cambridge University Press.
- WILLS, J. A. B. 1964 On convection velocities in turbulent shear flows. *J. Fluid Mech.* **20**, 417.



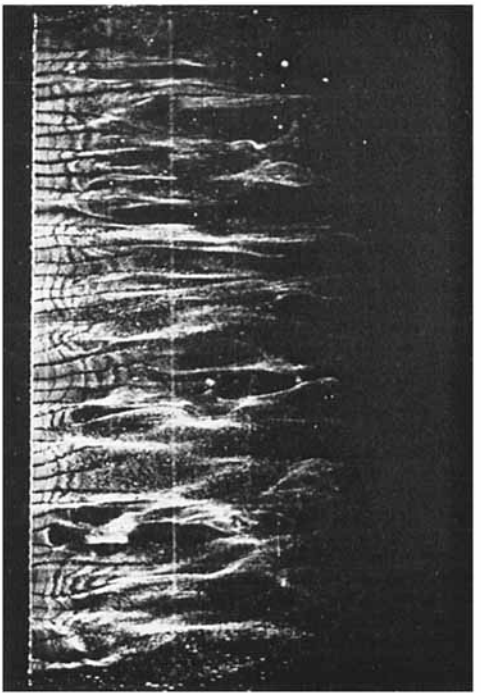
(b)



(d)



(a)



(c)

FIGURE 12. Hydrogen bubble visualization in the wall region of a boundary layer. From Kline *et al.* (1967).
(a) $y^+ = 2.7$; (b) $y^+ = 4.5$; (c) $y^+ = 6.6$; (d) $y^+ = 9.6$.

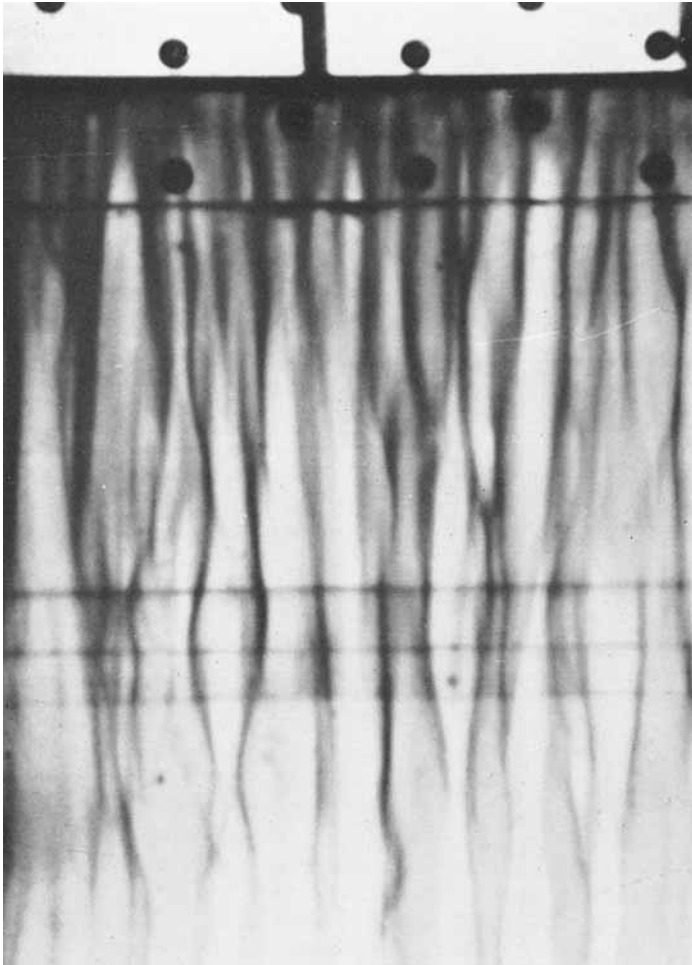


FIGURE 13. Dye filaments at the wall of a boundary layer. From Runstadler *et al.* (1963).